Workability and mechanical properties of alkali-activated fly ash-slag concrete cured at ambient temperature

Guohao Fang, Wing Kei Ho, Wenlin Tu, Mingzhong Zhang *

Advanced and Innovative Materials (AIM) Group, Department of Civil, Environmental and Geomatic Engineering, University College London, London WC1E 6BT, UK

HIGHLIGHTS

- Workability of alkali-activated fly ash-slag (AAFS) concrete measured.
- Mechanical properties of AAFS concrete measured.
- Effects of slag content, molarity of SH, AL/B ratio and SS/SH ratio estimated.
- Prediction equations for splitting tensile strength and flexural strength proposed.
- Optimal mixtures of AAFS concrete for engineering application obtained.

GRAPHICAL ABSTRACT
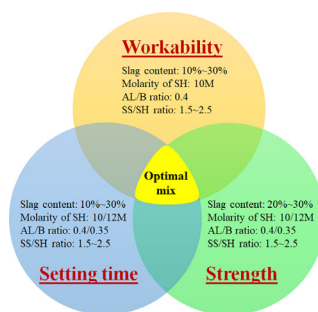
ABSTRACT

Alkali-activated fly ash-slag (AAFS) concrete is a new blended alkali-activated concrete that has been increasingly studied over the past decades because of its environmental benefits and superior engineering properties. However, there is still a lack of comprehensive studies on the effect of different factors on the fresh and hardened properties of AAFS concrete. This paper aims to provide a thorough understanding of workability and mechanical properties of AAFS concrete cured at ambient temperature and to obtain the optimal mixtures for engineering application. A series of experiments were carried out to measure workability, setting time, compressive strength, splitting tensile strength, flexural strength and dynamic elastic modulus of AAFS concrete. The results showed that workability and setting time decreased with the increase of slag content and molarity of sodium hydroxide solution (SH). Compressive strength increased with the increase of slag content and molarity of SH as well as the decrease of alkaline activator to binder (AL/B) ratio, but it did not have significant relationship with sodium silicate to sodium hydroxide (SS/SH) ratio. In addition, equations provided by ACI code, Eurocode and previous researchers for ordinary Portland cement concrete overestimated the values of splitting tensile strength, flexural strength and dynamic elastic modulus of AAFS concrete. The optimal mixtures of AAFS concrete were set as slag content of 20–30%, AL/B ratio of 0.4, 10 M of SH, and SS/SH ratio of 1.5–2.5 considering the performance criteria of workability, setting time and compressive strength.

1. Introduction

Alkali-activated materials (AAM) is an inorganic binder derived by the reaction of an alkali metal source (solid or dissolved) with a solid silicate powder such as fly ash (FA) and slag [1]. To date, AAM has been recognized as a promising alternative binder to ordinary Portland cement (OPC) because of its environmental benefits and superior engineering properties [2–5]. The manufacture of OPC is known as a significant contributor to greenhouse gas emissions accounting for around 5% of global CO_2 emissions [6,7]. In comparison, there are about 55–75% less greenhouse gas emissions in the

production of FA and slag [8]. Thus, the application of AAM as a binder can significantly reduce the CO_2 emissions of concrete production.

FA has been increasingly considered as a suitable raw material for alkali-activated concrete (AAC) due to its wide availability and adequate composition of silica and alumina. Previous studies [9–19] reported that alkali-activated fly ash (AAF) concrete has excellent mechanical and durability properties when it is cured at elevated temperature. Normally, the curing temperature of 60–85 °C is required to activate FA as the reactivity of FA at ambient temperature is too low to be activated by alkali activators [20–22]. Such curing condition may be suitable for manufacturing precast concrete members, but it is not suitable for cast-in-situ concrete in practice. Therefore, it is vital to develop a new type of AAC without curing at elevated temperature, which will widen the practical application of AAC. In addition, the cost and energy consumption associated with the heat curing process will also be reduced.

In order to achieve ambient curing, some researchers attempted to improve the reactivity of FA in alkaline environment [23]. In particular, one of the acceptable attempts is to add some calcium containing materials such as slag in AAC [24]. The addition of slag would accelerate FA dissolution and enhance reaction products formation in room curing condition [25]. Both the early and later age properties of AAF concrete are also significantly affected by the additional slag. Until now, an increasing number of studies have been undertaken to investigate the effect of slag on the engineering properties of AAF [2,3,26–30]. Nath and Sarker [2,3,31] studied the influencing factors on the fresh and hardened properties of alkali-activated fly ash-slag (AAFS) concrete. It was found that the dominant influencing factors are the slag replacement level for FA along with the type and content of alkaline activator. One main limitation of this research is that the different activating conditions were not fully considered. For example, the effect of slag content on the properties of AAFS concrete may be affected by the activator with different molarity. Lee [29,32] also explored the mechanical properties of AAFS concrete and suggested a proper slag content of 15–20% of total binder considering the setting time and compressive strength of AAFS concrete. However, it should be noted that the workability of AAFS concrete was not considered in the selection of slag content. In addition, an optimal mixture of AAFS concrete should not only include the slag replacement level but also the alkaline activator to binder (AL/B) ratio, molarity of sodium hydroxide (SH) solution and sodium silicate to sodium hydroxide (SS/SH) ratio, etc. Thus, it is of importance to conduct a comprehensive research focusing on the effects of different factors on the fresh and hardened properties of AAFS concrete and to evaluate the optimal mixtures by taking into account the basic performance criteria of workability, setting time and compressive strength.

The main purpose of this study is to provide a thorough understanding of workability, setting time and mechanical properties of AAFS concrete cured at ambient temperature. Low calcium FA and ground granulated blast-furnace slag (GGBS) were used as binder materials. Alkaline activator was prepared by mixing SH and SS solution. Special attention was paid to the main influencing factors, including FA/GGBS ratio, AL/B ratio, molarity of SH and SS/SH ratio on the workability, setting time, compressive strength, splitting tensile strength, flexural strength and dynamic elastic modulus

development of AAFS concrete. Splitting tensile strength, flexural strength and dynamic elastic modulus were further analysed using existing standards and codes in order to propose prediction equations suitable for AAFS concrete. Finally, the optimal mixtures of AAFS concrete were obtained based on the performance criteria of workability, setting time and compressive strength.

2. Experimental program

2.1. Materials

In this study, low calcium FA and GGBS were used as binder. The chemical compositions of FA and GGBS are listed in Table 1. The mean particle size of FA and GGBS is 26.81 and 14.77 μm, respectively. Alkaline activator (AL) was mixed by sodium hydroxide (SH) with distilled water and sodium silicate solution (SS). The SiO_2 to Na_2O ratio of SS was 2.0 with chemical composition of 30.71 wt% SiO_2, 15.36 wt% Na_2O and 53.93 wt% H_2O. Since the modified polycarboxylate-based superplasticizers (SPs) have a significant effect on the workability of AAFS [29], it was used to improve the workability of AAFS in this work. The properties of this SPs are given in Table 2. Natural sand with a nominal maximum size of 2 mm was used as the fine aggregate. Coarse aggregates (CA) were prepared by mixing crushed granite with nominal maximum sizes of 10 and 20 mm. Fine aggregates and coarse aggregates were used in saturated surface dry (SSD) condition according to ASTM C128-15 [33] and ASTM C127-15 [34], respectively.

2.2. Mixture proportions

AAFS specimens with different FA/GGBS ratio, AL/B ratio, molarity of SH and SS/SH ratio were prepared and tested in this work. The optimal scope of mixture proportions was selected according to the relevant studies [2,3,6,28,29,32]. The mix proportions of AAFS concrete are listed in Table 3 and labelled with specific codes. The labels 'A', 'B', 'C', and 'D' represent different specimen series, while the numbers, '10', '15', '20', '25' and '30', stand for the percentages of GGBS replacement for FA by weight, respectively. In Series A, mixture 1 (A10) to mixture 5 (A30) refer to those with GGBS content of 10%, 15%, 20%, 25% and 30% of total binder, respectively. The AL/B ratio in these mixtures was kept constant at 0.4 with molarity of SH and SS/SH ratio of 10 M and 2.0, respectively. In Series B, i.e., mixture 6 (B15) to mixture 8 (B25), the molarity of SH was changed from 10 M to 12 M while the AL/B ratio and SS/SH ratio were kept constant at 0.4 and 2.0, respectively. In Series C, i.e., mixture 9 (C15) to mixture 11 (C25), the AL/B ratio was changed from 0.4 to 0.35 while the molarity of SH and SS/SH ratio were kept as 10 M and 2.0, respectively. In Series D, the SS/SH ratios for mixture 12 (D15) and mixture 13 (D25) were 1.5 and 2.5, respectively. The SPs content was kept constant at 1% of the total binder for all mixtures. As such, the effect of slag content on the engineering properties of AAFS can be studied through Series A containing various slag content ranging from 10% to 30% of binder by weight. The effect of SH molarity can be investigated using Series A and Series B containing SH molarity of 10 and 12, respectively. Series A and Series C with AL/B ratios of 0.4 and 0.35 respectively were also designed to estimate the effect of AL/B ratio. Furthermore, Series A and Series D were conducted to evaluate the effect of SS/SH ratio on the engineering properties of AAFS with various SS/SH ratios ranging from 1.5 to 2.5.

The concrete mixtures were proportioned based on the unit volume of 1 m^3 while the total binder content was kept constant as 400 kg/m^3. The ingredient contents of binder were calculated based on their weight ratio. The total volume of aggregates was the residual volume except binder volume. The aggregates were mixed by the volume of 10 mm, 20 mm and fine aggregates with 22%, 43% and 35%, respectively. In addition, the mix proportions of AAFS pastes were similar to those of concrete mixtures excluding aggregates (see Table 3).

Table 2
Properties of superplasticizers.

Specific gravity (25 °C)	pH (25 °C)	Content of chloride ion (%)	Content of alkaline (%)
1.08	4–5	≤0.1	≤0.4

Table 1
Chemical compositions (wt%) of FA and GGBS.

Oxide	SiO_2	Al_2O_3	CaO	MgO	K_2O	Fe_2O_3	TiO_2	Na_2O	SO_3
FA	53.24	26.42	3.65	9.55	2.57	1.65	0.86	0.76	0.56
GGBS	36.77	13.56	37.60	7.45	0.55	0.41	0.79	0.25	1.82

Table 3
Mixtures of alkali-activated fly ash-slag concrete.

	Mix No.	Labels	Mixture proportions				Concrete mixture quantity (kg/m³)							
			FA/GGBS	AL/B ratio	Molarity of SH (M)	SS/SH ratio	FA	GGBS	SH	SS	SPs	Sand	CA 10 mm	CA 20 mm
A	1	A10	90/10	0.4	10	2	360	40	53	107	4	644	399	798
	2	A15	85/15	0.4	10	2	340	60	53	107	4	646	400	800
	3	A20	80/20	0.4	10	2	320	80	53	107	4	648	401	802
	4	A25	75/25	0.4	10	2	300	100	53	107	4	650	402	805
	5	A30	70/30	0.4	10	2	280	120	53	107	4	652	403	807
B	6	B15	85/15	0.4	12	2	340	60	53	107	4	646	400	800
	7	B20	80/20	0.4	12	2	320	80	53	107	4	648	401	802
	8	B25	75/25	0.4	12	2	300	100	53	107	4	658	407	815
C	9	C15	85/15	0.35	10	2	340	60	47	93	4	651	403	806
	10	C20	80/20	0.35	10	2	320	80	47	93	4	661	409	818
	11	C25	75/25	0.35	10	2	300	100	47	93	4	671	415	831
D	12	D15	85/15	0.4	10	1.5	340	60	64	96	4	637	395	789
	13	D25	75/25	0.4	10	2.5	300	100	46	114	4	659	408	815

Note: FA (Fly Ash); GGBS (Ground Granulated Blast-furnace Slag); SH (Sodium Hydroxide); SS (Sodium Silicate); SPs (Superplasticizers); CA (Coarse Aggregates).

2.3. Specimen preparation

The mixing method of AAFS concrete is presented as follows. FA, GGBS, fine aggregate and coarse aggregate were dry-mixed for 2 min to ensure homogeneity of the mixture. Then, AL and SPs were added into mixture and mixed for another 3 min. The fresh AAFS concrete was then immediately cast into three different moulds (cube with size of 100 mm for compressive test, cylinder with size of 100 × 200 mm for splitting tensile test and prism with size of 100 × 100×500 mm for four-point bending test and dynamic elastic modulus test). For each testing age, three specimens were prepared for each mixture. All specimens were then stored in a curing room (20 ± 2 °C, 60% ± 5% RH). After 24 h, the specimens were de-moulded and placed in curing room under the same environmental condition until the day of testing.

2.4. Testing methods

The workability of AAFS pastes was investigated using flow table test according to ASTM C230-14 [35], where the diameter of the paste spread in two directions at right angles was measured to calculate the flow value. Slump value as described in ASTM C143-15a [36] was conducted to determine workability of AAFS concrete, where vertical difference between the top of the mould and the displaced original centre of the top surface of the specimen was measured as the slump value. The initial and final setting time of AAFS pastes was determined by the Vicat setting test according to ASTM C191-08 [37]. AAFS paste was proportioned and mixed to normal consistency for the setting time test according to previous research [38]. Periodic penetration tests were performed by allowing a 1-mm Vicat needle to settle into this paste. The Vicat initial setting time was the time elapsed between the initial contact of raw materials and activator and the time when penetration was measured to be 25 mm. The Vicat final setting time was the time elapsed between initial contact of raw materials and activator and the time when the needle did not leave a complete circular impression in the paste surface. According to BS EN 12390-3:2009 [39], a universal testing machine was used to test the compressive strength of AAFS concrete at 1, 7, 14, 28 and 56 d, where the constant rate of loading was set as 5 kN/s. The splitting tensile strength of AAFS concrete at 7 and 28 d was tested according to ASTM C496-11 [40] at a loading rate of 0.6 kN/s. The flexural strength of AAFS concrete at 28 d was determined using four-point bending test according to ASTM C78-16 [41] at a loading rate of 40 N/s. The dynamic elastic modulus of AAFS concrete was determined according to ASTM C215-14 [42] at 7, 14, 21 and 28 d, where the fundamental longitudinal frequency along with the dimensions and mass of the specimen were used to calculate the dynamic elastic modulus.

3. Results and discussion

3.1. Workability

Generally, the workability of AAC is lower than that of OPC concrete because the presence of silicate in AAC would bring a sticky characteristic. Nevertheless, AAC can compact well on a vibrating table even for relatively low slump value. Therefore, the workability of AAC is classified based on the condition of compaction as shown below [43]. When AAC achieves a slump value of 90 mm and over, it is regarded as a highly workable concrete. AAC with the slump values in the range of 50 mm and 89 mm is classified as medium workability, while AAC with slump values below 50 mm is considered as low workability due to the significant vibration of compaction. Thus, in this study, this criterion was applied to identify the optimal mixture of AAFS concrete in terms of workability.

3.1.1. Effect of fly ash/slag ratio

Fig. 1 shows the flow value of AAFS pastes and slump value of AAFS concrete with various slag content. Both the flow value of AAFS pastes and the slump value of AAFS concrete were influenced by the replacement level of slag in binder. The slump and flow values decreased with the increase of slag content in the mixture, which is consistent with previous studies [2,3]. This can be attributed to the accelerated reaction of calcium and the angular shape of slag comparing with the spherical shape of fly ash particles [2]. However, the effect varied with the amount of slag. For Series A, the slump value of A15, A20, A25 and A30 decreased 5.40%, 17.50%, 24.62% and 25.91% respectively as compared to A10. For Series B, the slump decreasing value of B20 and B25 was 51.03% and 64.48% respectively as compared to B15. In Series C, the slump value of C20 and C25 was 6.96% and 14.55% lower than that of C15, respectively. The effect of slag at 20% replacement level appeared to be more pronounced. Moreover, it seems that the effect of slag content was more significant at higher molarity of SH (12 M) and higher AL/B ratio (0.4).

3.1.2. Effect of molarity of sodium hydroxide solution

Comparing the flow and slump values of Series A and Series B in Fig. 1, it can be found that the workability of AAFS decreased with the increase of SH molarity. All the slump value of 10 M specimens in Series A was higher than 171 mm, while the slump value of 12 M specimens in Series B was lower than 145 mm. This is mainly because that the increase of SH molarity increased the viscosity of the solution [44]. However, the effect of SH molarity varied with slag replacement ratio. The slump value of B15 (145 mm) was decreased by 74 mm compared with that of A15 (219 mm). When the replacement of slag reached 20% and 25%, the slump values of B20 (71 mm) and B25 (51.5 mm) were decreased by 120 mm and 123 mm respectively compared with the slump value of corresponding 10 M specimens in Series A. The effect of SH molarity was more obvious for the mixtures with a higher slag replacement level.

3.1.3. Effect of alkaline activator/binder ratio

As shown in Fig. 1, the mixtures with AL/B ratio of 0.35 (Series C) exhibited relatively low flow value and slump value as com-
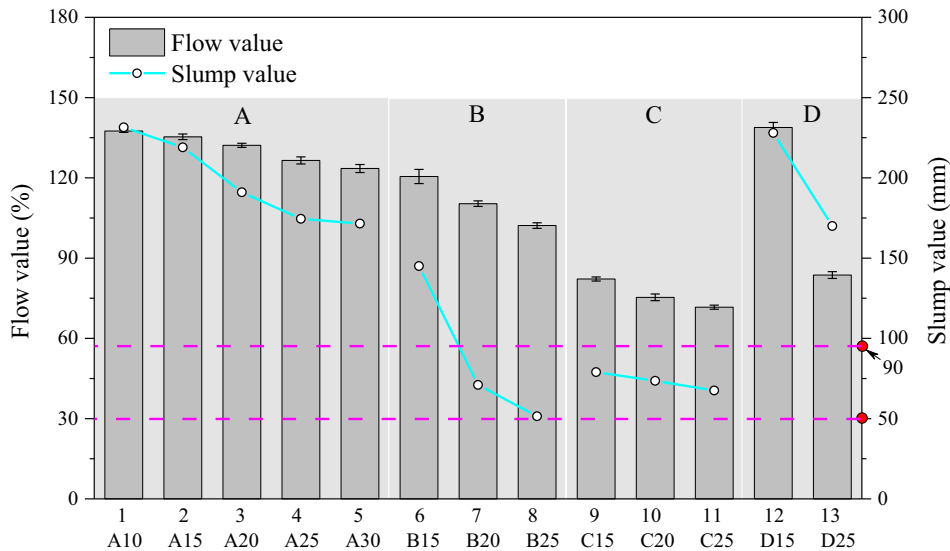
Fig. 1. Flow and slump values of alkali-activated fly ash-slag pastes and concrete.

pared to the mixtures in Series A with AL/B ratio of 0.4. The slump value of the specimens in Series C was in the range between 67 mm and 79 mm, while the slump value of Series A was much higher than that of Series C with a range from 171 mm to 231 mm. More specifically, the effect of AL/B ratio can be observed in the mixtures with different slag replacement levels. The slump value of C15 decreased 63.95% as compared to A15, while those of B20 and B25 decreased 61.51% and 61.31% as compared to A20 and A25, respectively. It is indicated that the alkaline activator content in the mixtures plays a dominant role in workability of AAFS concrete, which is consistent with other research [2,3].

3.1.4. Effect of sodium silicate/sodium hydroxide ratio

As shown in Fig. 1, the slump value of D15 (SS/SH ratio of 1.5) kept the highest level (228 mm). When the SS/SH ratio increased to 2.0, the slump value decreased to 219 mm (A15). Similarly, when the SS/SH ratio increased from 2.0 to 2.5, the slump value (174.5 mm) of A25 decreased to 170 mm (D25). It indicates that the workability of AAFS concrete decreased with the increase of SS/SH ratio, which is in good agreement with previous research [2,3]. Since SS is the most viscous solution in the alkaline liquid, with the increase of SS/SH ratio from 1.5 to 2.5 the viscosity of AAFS mixture tends to increase resulting in a lower workability [2,3,45].

3.1.5. Optimal mixtures in terms of workability

According to the classification of AAC workability as mentioned above, the mixtures were divided into three different categories (see Fig. 1). For Series A, all AAFS mixtures can be classified as highly workable concrete as the slump value of these specimens was higher than 90 mm. For Series B, only mixture 6 (B15) was defined as highly workable concrete, while other two mixtures were classified as medium workable concrete. Furthermore, all the mixtures in Series C were classified as medium workable concrete because the slump value of these mixtures were in the range between 50 and 90 mm. For Series D, all the mixtures were considered as highly workable concrete according to the classification. Therefore, the mixtures with a slag replacement level from 10% to 30%, AL/B ratio of 0.4, 10 M of SH, and SS/SH ratio in the range of 1.5–2.5 can be suggested as optimal mixtures for the sake of workability.

3.2. Setting time

Setting time is one of the important properties of concrete. It can be divided into initial setting time and final setting time based on the degree of rigidity. According to ASTM C403-08 [46], the initial and final setting time can be determined as the time when the penetration resistance equals to 3.5 MPa and 27.6 MPa, respectively. According to BS EN 197-1:2011 [47], the initial setting time of OPC with strength class of 42.5 should be longer than 60 min. In this study, this criterion was used to verify the feasibility of AAFS concrete in terms of setting time.

3.2.1. Effect of fly ash/slag ratio

Fig. 2 shows the variation of setting time of AAFS pastes with different slag content. Both the initial and final setting time of AAFS pastes decreased with the increase of slag replacement level. High initial and final setting time of specimens with 10% slag replacement can be found. When more slag was added into the mixtures the initial setting time was reduced significantly from 350 min to 77–118 min, while the final setting time was decreased from 470 min to 107–128 min. The initial setting time of A15, A20, A25 and A30 was found to be reduced by 18.57%, 62.85%, 63.14% and 65.71% and the final setting time was reduced by 31.91%, 63.83%, 64.04% and 70.21% compared to the setting time of A10, respectively. The reducing percentage of setting time was higher for the specimens with higher slag content. This is mainly ascribed to the corresponding higher amount of reactive slag, which contributes to the formation of C-A-S-H gel along with N-A-S-H gel at early duration, as such the reaction process is accelerated [24]. In addition, the effect of slag content seemed more significant at higher molarity of SH (12 M) and higher AL/B ratio (0.4).

3.2.2. Effect of molarity of sodium hydroxide solution

As shown in Fig. 2, the 10 M specimen with 15% slag (A15) had an initial setting time of 285 min and final setting time of 320 min, while the 12 M specimen (B15) had a relatively higher initial setting time of 320 min and final setting time of 400 min. Similarly, for the specimens with 20% slag (A20 and B20), the initial setting time was found to be increased from 130 min to 183 min and the final setting time was increased from 170 min to 213 min with the increase of SH molarity from 10 M to 12 M. However, increasing the SH molarity in specimens with 25% slag (A25 and B25)
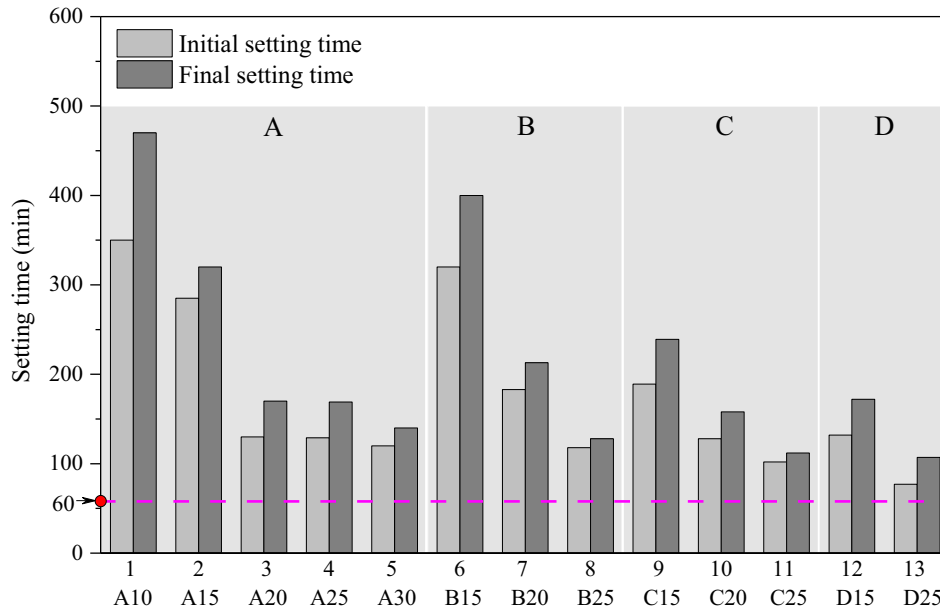
Fig. 2. Setting time of alkali-activated fly ash-slag pastes.

reduced the initial setting time from 129 min to 118 min and the final setting time from 169 min to 128 min. It indicated that the setting time increased with the increase of molarity of SH except for the specimens with 25% slag. Generally, with the increase of SH molarity in the mixtures the setting time is decreased if only SH is used as alkaline activator. This is because it would increase the hydroxide ion concentration and accelerate the dissolution of raw materials [21]. Nevertheless, a mix solution composed of SS and SH was used as activator. It means that increasing the SH molarity would also affect the silica modulus (molar ratio of SiO_2/Na_2O) of the alkaline liquid, which would influence the alkaline activation process. In this study, the modulus of mixtures in Series A was decreased from 1.13 to 1.04 when the SH molarity was increased from 10 M to 12 M. Normally, a higher modulus of alkaline solution would accelerate the alkaline activation process and reduce the setting time [48]. Thus, this may be the reason why increasing the SH molarity would increase the setting time.

3.2.3. Effect of alkaline activator/binder ratio

Series A and Series C in Fig. 2 represents the setting time of specimens with AL/B ratio of 0.4 and 0.35, respectively. When the AL/B ratio was reduced from 0.4 to 0.35, the range of initial setting time was decreased from 129 to 285 min to 102–189 min and the final setting time was reduced from 169 to 320 min to 112–239 min. It indicated that a lower AL/B ratio led to a shorter setting time because of the decrease of total liquid content. According to previous research, the reduction of AL/B ratio would decrease the consistency of AAFS concrete, which would result in the accelerated reaction of raw materials [49].

3.2.4. Effect of sodium silicate/sodium hydroxide ratio

As the SS/SH ratio increased from 1.5 to 2.5, the setting time of specimens was significantly affected (see Series D in Fig. 2). For the mixtures with 15% slag (i.e. A15 and D15), the initial setting time of AAFS pastes was found to be reduced from 285 min to 132 min and the final setting time was reduced from 320 min to 172 min when the SS/SH ratio was decreased from 2.0 to 1.5. However, the initial and final setting time was decreased with the increase of SS/SH ratio from 2.0 to 2.5 (see A25 and D25 in Fig. 2). The different effect of SS/SH ratio on setting time may be attributed to the interaction

between SS and SH [32]. Thus, more information (e.g. the silica modulus of alkaline solution) is required to discuss this interaction mechanism. According to the mix proportion, the solution moduli of mixtures with three different SS/SH ratios, including 1.5 (D15), 2.0 (A15 and A25) and 2.5 (D25) were calculated to be 0.99, 1.13 and 1.9, respectively. There is not much difference between the moduli of A15 and D15, which means that the dissolute silica content may be not the main reason to explain why the setting time decreased with the decrease of SS/SH ratio from 2.0 to 1.5. Thus, the main reason may be attributed to the increase of relative amount of SH. Increasing the amount of SH increases the hydroxide ion concentration in mixtures, which would accelerate dissolution of raw materials and thus reduce setting time [50]. On the other hand, the modulus of D25 (1.9) is much higher than that of A25 (1.13), which indicates that the dissolute silica content was increased with the increase of SS/SH ratio from 2.0 to 2.5. Thus, the decrease of setting time with the increase of SS/SH ratio from 2.0 to 2.5 may be ascribed to the dissolute silica content. A higher content of dissolute silica would enhance the alkali activation process and reduce the time to complete the dissolution reaction resulting in the decrease of setting time [48].

3.2.5. Optimal mixtures in terms of setting time

As shown in Fig. 2, the initial setting time of all mixtures is longer than 60 min, which can fulfil the setting time requirement of BS EN 197-1:2011 [47]. Thus, the chosen parameters in this work (i.e., slag replacement level from 10% to 30%, AL/B ratio of 0.4 and 0.35, 10 M and 12 M of SH, and SS/SH ratio in the range of 1.5–2.5) are suitable for the AAFS in terms of setting time. However, it should be mentioned that the performance criteria would be varied according to different engineering application.

3.3. Compressive strength

Compressive strength is one of the most important mechanical properties of concrete. According to ACI 318 M-05 [51], the 28-d compressive strength of concrete need to achieve at least 28 MPa for the basic engineering application. For the corrosion protection of reinforcement in concrete, the minimum compressive strength of concrete is 35 MPa. In this study, these criteria were used to

identify the optimal mixtures of AAFS concrete in terms of compressive strength.

3.3.1. Effect of fly ash/slag ratio

Fig. 3 shows the compressive strength of AAFS specimens with different slag replacement levels. It can be seen that the development of compressive strength follows the similar trends but different magnitudes. The compressive strength of AAFS concrete increased dramatically at early 28 d but after that the increasing rate of compressive strength became slower. In addition, the compressive strength of AAFS concrete increased with the amount of slag. For instance, when the slag replacement level was increased from 10% to 30%, the 28-d compressive strength was increased from 21.90 to 56.43 MPa. This can be attributed to the formation of C-A-S-H gels, which would reduce the porosity and condense the microstructure of AAFS matrix [24,52–55]. Furthermore, the effect of slag at 20% replacement level on the increase of compressive strength appeared to be more pronounced. For example, the 28-d compressive strength of specimens was increased by 34.29%, 90.70%, 113.44% and 157.66% with every 5% increment of slag content from 15% to 30% when compared to the specimen with 10% slag (A10).

3.3.2. Effect of molarity of sodium hydroxide solution

Fig. 4 shows the effect of molarity of SH on compressive strength of AAFS concrete. It can be noted that increasing the molarity of SH from 10 M (series A) to 12 M (series B) gradually increased the compressive strength of AAFS concrete, which can be explained by the reaction of the internal Si, Al and Ca components caused by the increased breakage of the T-O-T bonds (T: Si or Al) in FA and Ca-O and Si-O bonds in GGBS provoked by the high alkalinity resulting from the increasing molarity of SH [56,57]. The 28-d compressive strength of AAFS concrete with 15% slag (B15) was increased by 23.08% as compared to that of A15. The 28-d compressive strength of B25 was increased by 23.19% as compared to that of A25, while the effect was less pronounced for B20, the 28-d compressive strength of which was increased by 10.96% compared to that of A20.

3.3.3. Effect of alkaline activator/binder ratio

Fig. 5 shows the compressive strength of AAFS concrete with different alkaline activator to binder ratios. It was found that
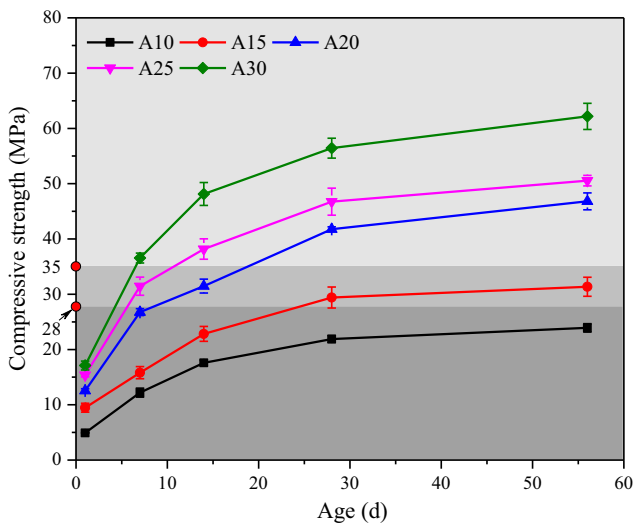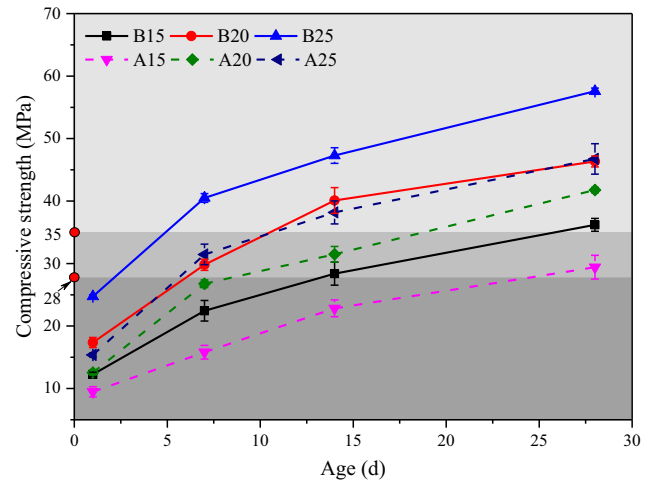

Fig. 4. Compressive strength of alkali-activated fly ash-slag concrete with different molarity of sodium hydroxide solution.

decreasing the AL/B ratio from 0.4 (Series A) to 0.35 (Series C) increased the compressive strength of concrete. The difference of compressive strength between specimens with different AL/B ratios became larger with the increase of curing age from 1 to 14 d. However, after that the difference become smaller and the compressive strength at 28 d was almost the same. Thus, it can be said that the amount of AL would strongly affect the early-age (<14 d) compressive strength of AAFS concrete, but no significant effect on the 28-d compressive strength. According to previous research, the alkaline activation process of AAFS would be accelerated with the decrease of AL/B ratio due to the decrease of consistency of mixtures [49]. In this case, the reaction products such as C-A-S-H gel and N-A-S-H gel can be produced quickly in the mixtures with low AL/B ratio and contribute to the development of early-age compressive strength (from 1 to 14 d in this study) [24,52]. Nevertheless, the reaction rate became slow after 14 d because most of the raw materials have been reacted.

3.3.4. Effect of sodium silicate/sodium hydroxide ratio

Fig. 6 shows the compressive strength of AAFS concrete with different SS/SH ratios of 1.5 (D15), 2.0 (A15 and A25) and 2.5
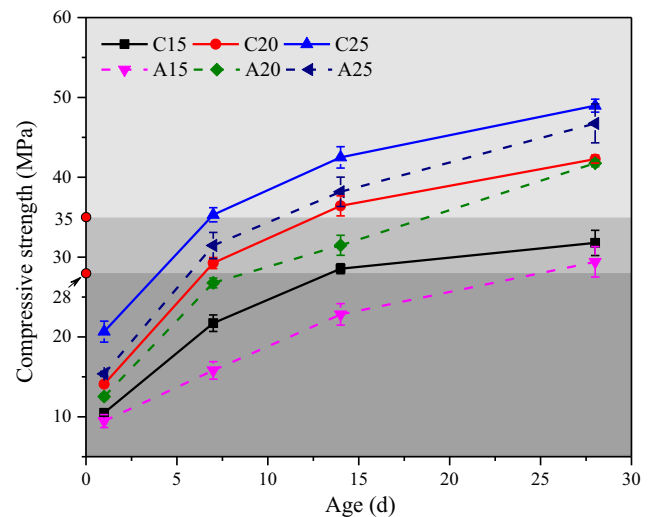

Fig. 3. Compressive strength of alkali-activated fly ash-slag concrete with different slag content.

Fig. 5. Compressive strength of alkali-activated fly ash-slag concrete with different alkaline activator to binder ratios.
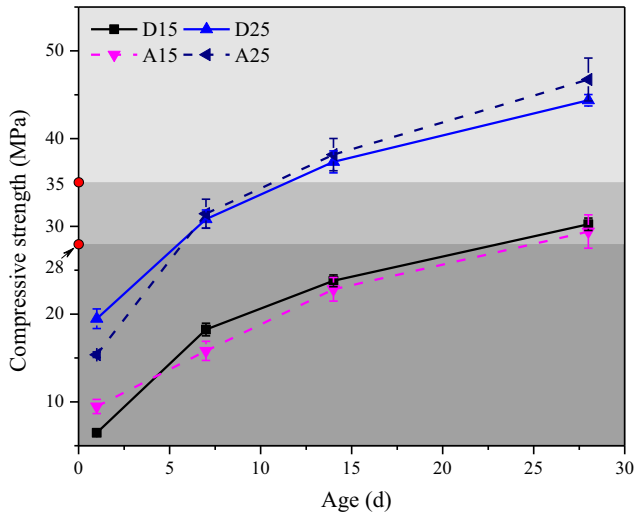
Fig. 6. Compressive strength of alkali-activated fly ash-slag concrete with different sodium silicate to sodium hydroxide ratios.

(D25). Comparing the corresponding graphs for same slag replacement level in Series A and Series D, it can be seen that the effect of SS/SH ratio on the compressive strength of AAFS concrete was not obvious. The 1-d compressive strength of AAFS concrete was increased slightly with the increase of SS/SH ratio, while the compressive strength of AAFS concrete with low SS/SH ratio was slightly higher than that of specimens with high SS/SH ratio at later age. This phenomenon was also found by Nath and Sarker [3].

3.3.5. Optimal mixtures in terms of compressive strength

As shown in Figs. 3–6, the 28-d compressive strengths of all mixtures except the mixtures with 10% slag are higher than 28 MPa and satisfy the basic requirement of normal concrete. However, for the application of reinforced concrete, only mixtures with relatively high slag content (≥20%) can meet the performance criteria because they can achieve a 28-d compressive strength of 35 MPa and more. Therefore, the mixtures with slag replacement level from 20% to 30%, AL/B ratio from 0.35 to 0.4, 10 M and 12 M of SH, and SS/SH ratio in the range of 1.5–2.5 can be suggested as optimal mixtures for the sake of compressive strength.

3.4. Splitting tensile strength

Splitting tensile strength of concrete is an important mechanical property, which is related to some aspects of concrete structures such as initiation and propagation of cracks, shear and anchorage of reinforcing steel in concrete. Generally, the splitting tensile strength of concrete can be predicted based on its compressive strength. ACI 318-05 [51] and Eurocode 2 [58] are commonly used to predict the splitting tensile strength of OPC concrete, according to which the splitting tensile strength of concrete can be calculated from the compressive strength using Eqs. (1) and (2), respectively.

$$f_{ct} = 0.56\sqrt{f'_c} \tag{1}$$

$$f_{ct} = \left(\frac{1}{3}\right)(f_c)^{2/3} \; for \; f_c < 50 \, \text{MPa} \tag{2}$$

where f_{ct} is the splitting tensile strength (MPa), f'_c is the specified compressive strength (MPa) and f_c is the average compressive strength (MPa).

For AAFS concrete, it was found that most of the measured splitting tensile strengths were lower than those predicted by the ACI 318-08 and Eurocode 2 [32,59]. Lee and Lee [32] observed that the splitting tensile strength of AAFS concrete had a linear relationship with the square root of the compressive strength, as shown in Eq. (3). Similarly, Sofi et al. [59] found that the linear relationship between splitting tensile strength and square root of compressive with the constant of 0.48 (Eq. (4)), which was slightly higher than the fitting results proposed by Lee and Lee [32].

$$f_{ct} = 0.45\sqrt{f'_c} \tag{3}$$

$$f_{ct} = 0.48\sqrt{f'_c} \tag{4}$$

As shown in Fig. 7, however, the measured splitting tensile strength in this study was lower than the predictions by the ACI 318-05, Eurocode 2, Lee and Sofi et al. [32,59]. However, it is worth pointing out that the predicted relationship between splitting tensile strength and compressive strength of AAFS concrete is strongly affected by many influencing factors, such as chemical and physical properties of raw materials and type of alkaline activators. The splitting tensile strengths of AAFS concrete at 7 and 28 d are plotted in Fig. 8. The splitting tensile strength increased with the increase of curing age for all mixtures. As seen in Series A, the splitting tensile strength of AAFS concrete increased with the increase of slag content and was also affected by the molarity of SH in mixtures. When the molarity of SH was increased from 10 M (Series A) to 12 M (Series B), the splitting tensile strength of AAFS concrete was improved. Furthermore, comparing the corresponding graphs for same slag replacement level in Series A and Series C, it can be observed that the 7-d splitting tensile strength increased with the decrease of AL/B ratio from 0.4 to 0.35. However, the 28-d splitting tensile strengths of mixtures with AL/B ratio of 0.35 (Series C) were smaller than those of mixtures with AL/B ratio of 0.4 (Series A). It is indicated that AL/B ratio would strongly affect the early-age splitting tensile strength development of AAFS concrete, but less significantly at the development of later-age splitting tensile strength. The influences of FA/GGBS ratio, SH molarity and AL/B ratio on the splitting tensile strength are similar to those on compressive strength. However, for the effect of SS/SH ratio on splitting tensile strength, the developing trend was different as compared to
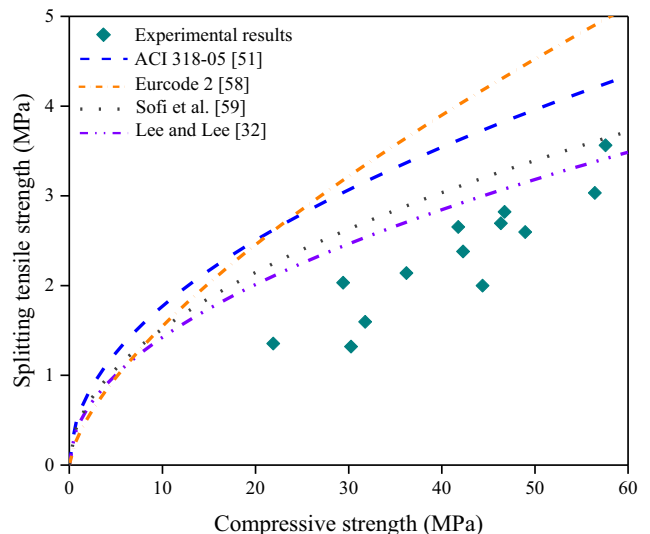

Fig. 7. Comparison of experimental and predicted splitting tensile strength of alkali-activated fly ash-slag concrete at 28 d.
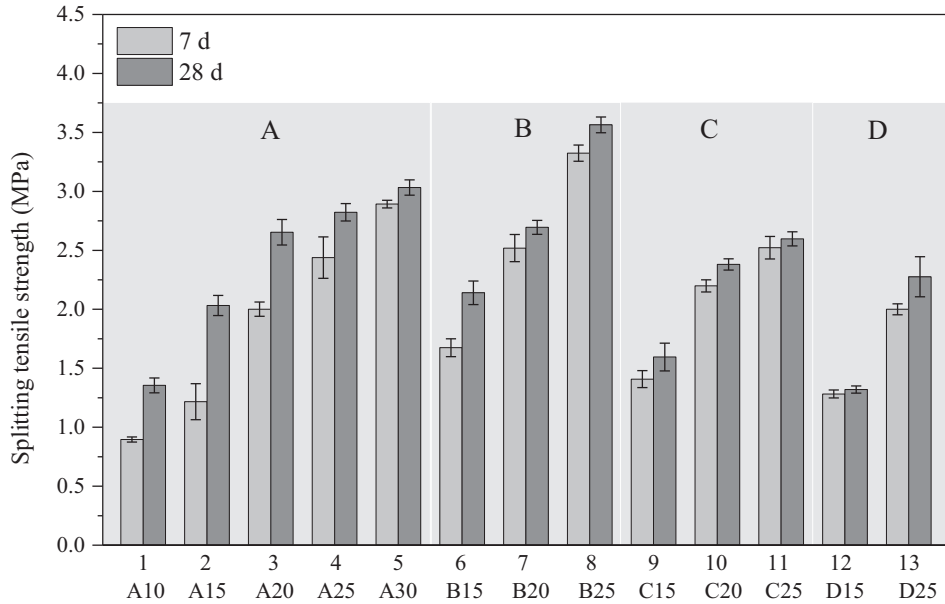
Fig. 8. Splitting tensile strength of alkali-activated fly ash-slag concrete at 7 d and 28 d.

that on compressive strength. The splitting tensile strength increased with the increase of SS/SH ratio from 1.5 (D15) to 2.0 (A15), while the splitting tensile strength decreased when the SS/SH ratio increased from 2.0 (A25) to 2.5 (D25).

3.5. Flexural strength

Flexural strength of concrete is another key mechanical property, which represents the ability of a beam or slab to resist failure in bending. Normally, the flexural strength of concrete has a strong relationship with its compressive strength. The flexural strength of OPC concrete, f_{ctf}, is commonly predicted using the ACI 318-05 [51] as

$$f_{ctf} = 0.62\sqrt{f'_c} \tag{5}$$

Similarly, some equations were proposed to predict the flexural strength of AAFS concrete. The relationship between flexural strength (f_{ctf}) and compressive strength (f_c) of AAF concrete can be expressed as $f_{ctf} = 0.69\sqrt{f_c}$ as suggested by Diaz-Loya et al. [60]. Nath and Sarker [31] also proposed an equation ($f_{ctf} = 0.93\sqrt{f_c}$) to predict the flexural strength of AAFS concrete.

The experimental and predicted value are plotted in Fig. 9. The flexural strength of AAFS concrete calculated using the equations proposed by Diaz-Loya et al. [60] and Nath and Sarker [31] was higher than measured values in this study, while the flexural strength of concrete predicted by ACI 318-05 was closer to measured values. Nevertheless, it should be highlighted that a general relationship between flexural strength and compressive strength of AAFS concrete is required due to limited available data and variability of mixture composition of AAFS concrete.

It can be seen from Fig. 10 that the 28-d flexural strength of AAFS concrete increased with the increase of slag content. Comparing the corresponding graphs for same slag content in Series A and Series B, the flexural strength of AAFS concrete increased significantly when the molarity of SH was increased from 10 M (Series A) to 12 M (Series B). As seen in Series A and Series C, the flexural strength of AAFS concrete increased dramatically with the decrease of AL/B ratio from 0.4 (Series A) to 0.35 (Series C). The effect of SS/
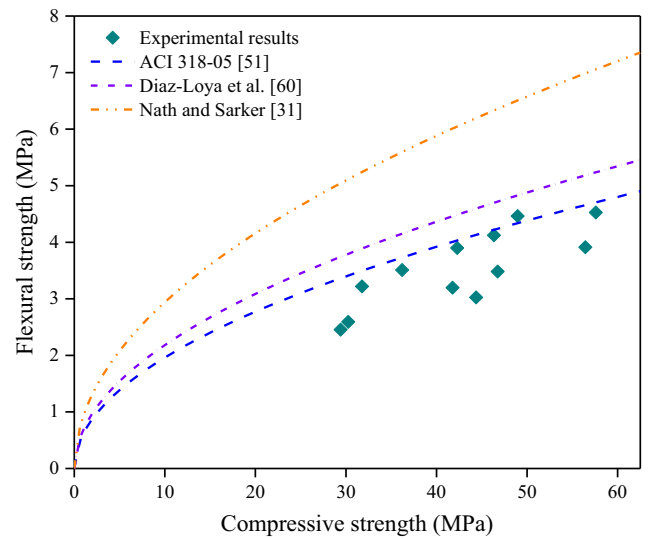

Fig. 9. Comparison of experimental and predicted flexural strength of alkali-activated fly ash-slag concrete at 28 d.

SH ratio on flexural strength of AAFS concrete was not significant, as seen in Series A and Series D. These phenomena are similar to the results shown in the development of compressive strength.

3.6. Dynamic elastic modulus

Dynamic elastic modulus is a mechanical property of viscoelastic material, which is defined as the ratio of stress to strain when the material is undertaking dynamic loading. According to the CEB-FIP model code [61] and the British testing standard BS8100 Part 2 [62], the dynamic elastic modulus of OPC concrete can be calculated by Eqs. (6) and (7).

$$E_c = 22(f_c/10)^{0.3} \tag{6}$$
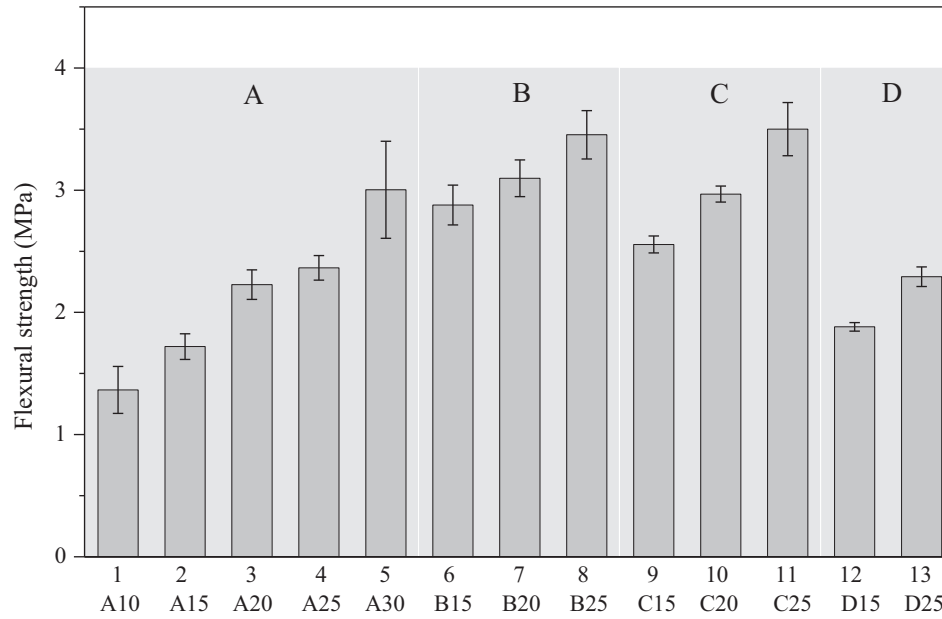
$$E_d = \frac{E_c + 19}{1.25} \tag{7}$$

Fig. 10. Flexural strength of alkali-activated fly ash-slag concrete at 28 d.

where E_c is the static elastic modulus (GPa), E_d denotes the dynamic elastic modulus (GPa) and f_c is the compressive strength (MPa).

An empirical relationship between dynamic elastic modulus and compressive strength of OPC concrete, $E_d = 14.72(f_c)^{0.3} - 9.56$, was also proposed by Zhou et al. [63]. In addition, Noguchi et al. [64] proposed an equation, $E_d = 12.66(f_c)^{0.27}$, to predict the dynamic elastic modulus of OPC concrete.

The experimental and measured values are plotted in Fig. 11, which shows that the predicted dynamic elastic modulus using equations proposed by Zhou et al. [63] and Noguchi et al. [64] was obviously higher than the measured values. The predicted data using Eqs. (6) and (7) were also higher than the measured data for
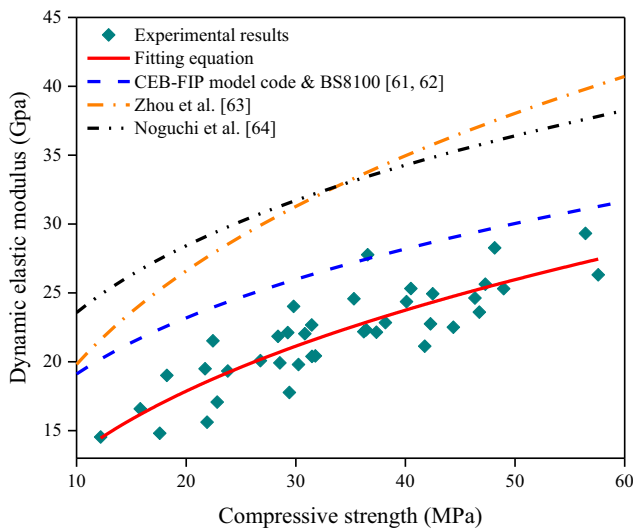
AAFS concrete. Thus, a more suitable equation, $E_d = 7.64(f_c)^{0.35} - 3.75$, was proposed here to predict the dynamic elastic modulus of AAFS concrete. Nevertheless, more experimental data are required to accurately predict the relationship between dynamic elastic modulus and compressive strength of AAFS concrete.

The dynamic elastic modulus of AAFS concrete with different mix proportions is plotted in Fig. 12. As seen in Fig. 12a, the dynamic elastic modulus of AAFS concrete steadily increased with the increase of slag replacement level. As the SH molarity increased from 10 M (Series A) to 12 M (Series B), the dynamic elastic modulus increased dramatically (see Fig. 12b). Furthermore, the dynamic elastic modulus of AAFS concrete would also be affected by AL/B ratio (see Fig. 12c). With the decrease of AL/B ratio from 0.4 (Series A) to 0.35 (Series C), the dynamic elastic modulus increased significantly. These phenomena can also be found in the developing trend of compressive strength. However, the effect of SS/SH ratio on dynamic elastic modulus is different from that on compressive strength. As shown in Fig. 12d, the dynamic elastic modulus of AAFS concrete decreased with the increase of SS/SH ratio from 1.5 (A15) to 2.0 (D15, and from 2.0 (A25) 2.5 (D25), respectively.

3.7. Optimal mixtures

Fig. 13 shows the obtained optimal mixtures of AAFS concrete according to the performance criteria of workability, setting time and compressive strength. Based on the discussion mentioned above, the optimal AAFS mixtures should have high workability (i.e., achieving a slump value of 90 mm or over) [43], suitable setting time (i.e., minimum initial setting time of 60 min) [47] and high compressive strength (i.e., minimum 28-d compressive strength of 35 MPa) [51]. Therefore, the mixtures with slag replacement level from 20% to 30%, AL/B ratio of 0.4, 10 M of SH, and SS/SH ratio in the range of 1.5 to 2.5 were suggested as optimal mixtures.
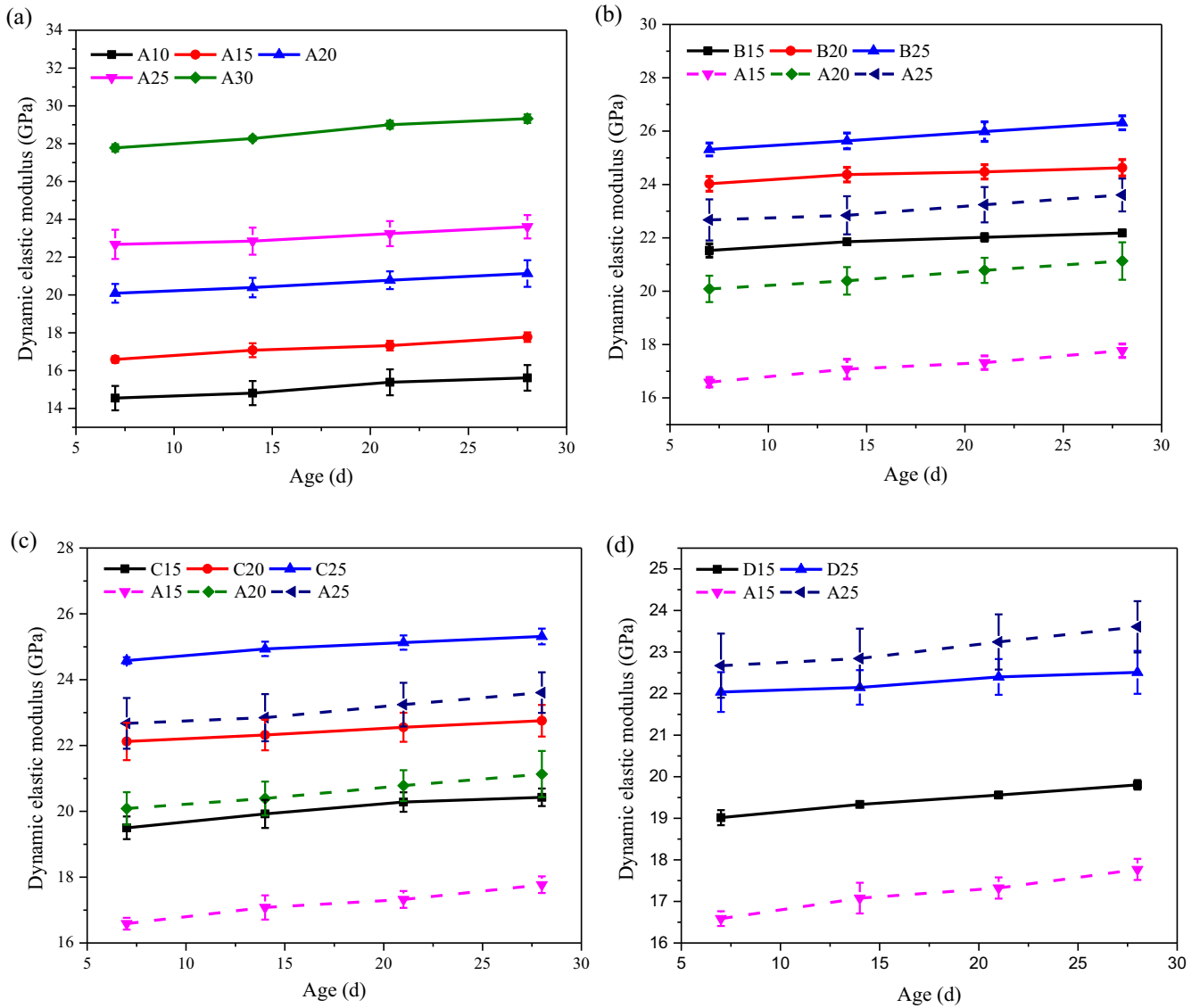

Fig. 11. Comparison of experimental and predicted dynamic elastic modulus of alkali-activated fly ash-slag concrete.

Fig. 12. Dynamic elastic modulus of alkali-activated fly ash-slag concrete with (a) different slag content, (b) different molarity of sodium hydroxide solution, (c) different alkaline activator to binder ratios, and (d) different sodium silicate to sodium hydroxide ratios.
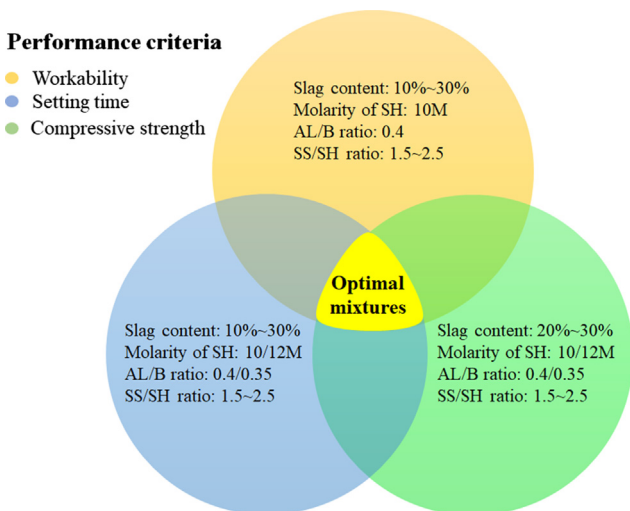

Fig. 13. Schematic illustration of optimal mixtures of alkali-activated fly ash-slag concrete in terms of workability, setting time and compressive strength.

4. Conclusions

In this study, the workability, setting time and mechanical properties of AAFS with different slag content, AL/B ratio, molarity of SH and SS/SH ratio were investigated. Afterwards, the optimal mixtures of AAFS were proposed. Based on the experimental results, the main conclusions can be drawn as follows:

- Workability of AAFS decreased with the increase of slag content and molarity of SH, as well as the decrease of AL/B ratio. The influence of slag content seemed more significant at higher molarity of SH and higher AL/B ratio. The specimens with higher molarity of SH at higher slag replacement level exhibited a more significant loss of workability than specimens with lower slag content.
- Setting time of AAFS pastes decreased with increasing slag content and decreasing AL/B ratio. The effect of slag at 20% replacement level on setting time appeared to be more pronounced.
- Compressive strength of AAFS increased significantly with the increase of slag content and molarity of SH as well as the decrease of AL/B ratio. The effect of slag content at 20% was

more significant, while the effect of SH molarity was less pronounced at slag replacement level of 20%. In addition, the amount of AL would significantly affect the compressive strength development at early age (<14 d), but the effect became less significant for the specimens at older age (28 d).

- Existing equations provided by ACI code, Eurocode and other researchers for OPC concrete overestimated the values of splitting tensile strength, flexural strength and dynamic elastic modulus of AAFS concrete. These mechanical properties of AAFS concrete cured at ambient temperature mostly followed a similar development trend as compressive strength.

- The mixtures of AAFS with slag replacement level from 20% to 30%, AL/B ratio of 0.4, 10 M of SH, and SS/SH ratio in the range of 1.5 to 2.5 can be suggested as optimal mixtures regarding the performance criteria of workability, setting time and compressive strength.

Conflict of interest

There is no conflict of interest.

Acknowledgements

References

[1] J. Provis, J.V. Deventer, Alkali activated materials: State-of-the-art report, RILEM TC 224-AAM Springe Netherlands (2014).

[2] P.S. Deb, P. Nath, P.K. Sarker, The effects of ground granulated blast-furnace slag blending with fly ash and activator content on the workability and strength properties of geopolymer concrete cured at ambient temperature, Mater. Des. 62 (2014) 32–39.

[3] P. Nath, P.K. Sarker, Effect of GGBFS on setting, workability and early strength properties of fly ash geopolymer concrete cured in ambient condition, Constr. Build. Mater. 66 (2014) 163–171.

[4] X. Fan, M. Zhang, Experimental study on flexural behaviour of inorganic polymer concrete beams reinforced with basalt rebar, Compos. B Eng. 93 (2016) 174–183.

[5] X. Fan, M. Zhang, Behaviour of inorganic polymer concrete columns reinforced with basalt FRP bars under eccentric compression: an experimental study, Compos. B Eng. 104 (2016) 44–56.

[6] Y. Ding, J.-G. Dai, C.-J. Shi, Mechanical properties of alkali-activated concrete: a state-of-the-art review, Constr. Build. Mater. 127 (2016) 68–79.

[7] C.D. Lawrence, The Production of Low-Energy Cements A2 - Hewlett, Peter C, Lea's Chemistry of Cement and Concrete, fourth ed., Butterworth-Heinemann, Oxford, 1998, pp. 421–470.

[8] K.-H. Yang, J.-K. Song, K.-I. Song, Assessment of CO_2 reduction of alkali-activated concrete, J. Cleaner Prod. 39 (2013) 265–272.

[9] P. Duxson, J.L. Provis, G.C. Lukey, J.S.J. van Deventer, The role of inorganic polymer technology in the development of 'green concrete', Cem. Concr. Res. 37 (12) (2007) 1590–1597.

[10] W.D.A. Rickard, J. Temuujin, A. van Riessen, Thermal analysis of geopolymer pastes synthesised from five fly ashes of variable composition, J. Non-Cryst. Solids 358 (15) (2012) 1830–1839.

[11] A. Fernandez-Jimenez, I. García-Lodeiro, A. Palomo, Durability of alkali-activated fly ash cementitious materials, J. Mater. Sci. 42 (9) (2007) 3055–3065.

[12] X.Y. Zhuang, L. Chen, S. Komarneni, C.H. Zhou, D.S. Tong, H.M. Yang, W.H. Yu, H. Wang, Fly ash-based geopolymer: clean production, properties and applications, J. Cleaner Prod. 125 (2016) 253–267.

[13] M.T. Junaid, A. Khennane, O. Kayali, A. Sadaoui, D. Picard, M. Fafard, Aspects of the deformational behaviour of alkali activated fly ash concrete at elevated temperatures, Cem. Concr. Res. 60 (2014) 24–29.

[14] X. Guo, H. Shi, W.A. Dick, Compressive strength and microstructural characteristics of class C fly ash geopolymer, Cem. Concr. Compos. 32 (2) (2010) 142–147.

[15] F. Pacheco-Torgal, Z. Abdollahnejad, A.F. Camões, M. Jamshidi, Y. Ding, Durability of alkali-activated binders: a clear advantage over Portland cement or an unproven issue?, Constr Build. Mater. 30 (2012) 400–405.

[16] M.T. Junaid, A. Khennane, O. Kayali, Performance of fly ash based geopolymer concrete made using non-pelletized fly ash aggregates after exposure to high temperatures, Mater. Struct. 48 (10) (2015) 3357–3365.

[17] J.G.S. van Jaarsveld, J.S.J. van Deventer, G.C. Lukey, The effect of composition and temperature on the properties of fly ash- and kaolinite-based geopolymers, Chem. Eng. J. 89 (1) (2002) 63–73.

[18] A.S. de Vargas, D.C.C. Dal Molin, A.C.F. Vilela, F.J.D. Silva, B. Pavão, H. Veit, The effects of Na_2O/SiO_2 molar ratio, curing temperature and age on compressive strength, morphology and microstructure of alkali-activated fly ash-based geopolymers, Cem. Concr. Compos. 33 (6) (2011) 653–660.

[19] M. Talha Junaid, O. Kayali, A. Khennane, Response of alkali activated low calcium fly-ash based geopolymer concrete under compressive load at elevated temperatures, Mater. Struct. 50 (1) (2016) 50.

[20] Y. Fan, S. Yin, Z. Wen, J. Zhong, Activation of fly ash and its effects on cement properties, Cem. Concr. Res. 29 (4) (1999) 467–472.

[21] K. Somna, C. Jaturapitakkul, P. Kajitvichyanukul, P. Chindaprasirt, NaOH-activated ground fly ash geopolymer cured at ambient temperature, Fuel 90 (6) (2011) 2118–2124.

[22] F. Puertas, S. Martínez-Ramírez, S. Alonso, T. Vázquez, Alkali-activated fly ash/slag cements: strength behaviour and hydration products, Cem. Concr. Res. 30 (10) (2000) 1625–1632.

[23] A.M. Rashad, A comprehensive overview about the influence of different admixtures and additives on the properties of alkali-activated fly ash, Mater. Des. 53 (2014) 1005–1025.

[24] S. Kumar, R. Kumar, S.P. Mehrotra, Influence of granulated blast furnace slag on the reaction, structure and properties of fly ash based geopolymer, J. Mater. Sci. 45 (3) (2010) 607–615.

[25] S. Puligilla, P. Mondal, Role of slag in microstructural development and hardening of fly ash-slag geopolymer, Cem. Concr. Res. 43 (2013) 70–80.

[26] S. Saha, C. Rajasekaran, Enhancement of the properties of fly ash based geopolymer paste by incorporating ground granulated blast furnace slag, Constr. Build. Mater. 146 (2017) 615–620.

[27] P. Nath, P.K. Sarker, Fracture properties of GGBFS-blended fly ash geopolymer concrete cured in ambient temperature, Mater. Struct. 50 (1) (2016) 32.

[28] W.-C. Wang, H.-Y. Wang, M.-H. Lo, The fresh and engineering properties of alkali activated slag as a function of fly ash replacement and alkali concentration, Constr. Build. Mater. 84 (2015) 224–229.

[29] J.G. Jang, N.K. Lee, H.K. Lee, Fresh and hardened properties of alkali-activated fly ash/slag pastes with superplasticizers, Constr. Build. Mater. 50 (2014) 169–176.

[30] G. Fang, H. Bahrami, M. Zhang, Mechanism of autogenous shrinkage of alkali-activated fly ash-slag pastes cured at ambient temperature within 24 hours, Construction and Building Materials, under minor revision.

[31] P. Nath, P.K. Sarker, Flexural strength and elastic modulus of ambient-cured blended low-calcium fly ash geopolymer concrete, Constr. Build. Mater. 130 (2017) 22–31.

[32] N.K. Lee, H.K. Lee, Setting and mechanical properties of alkali-activated fly ash/slag concrete manufactured at room temperature, Constr. Build. Mater. 47 (2013) 1201–1209.

[33] ASTM C128-15, Standard Test Method for Relative Density (Specific Gravity) and Absorption of Fine Aggregate, ASTM International, West Conshohocken, PA, 2015.

[34] ASTM C127-15, Standard Test Method for Relative Density (Specific Gravity) and Absorption of Coarse Aggregate, ASTM International, West Conshohocken, PA, 2015.

[35] ASTM C230-14, Standard specification for flow table for use in tests of hydraulic cement, ASTM International, West Conshohocken, PA, 2014.

[36] ASTM C143-15a, Standard Test Method for Slump of Hydraulic-Cement Concrete, ASTM International, West Conshohocken, PA, 2015.

[37] ASTM C191-08, Standard Test Methods for Time of Setting of Hydraulic Cement by Vicat Needle, American Society for Testing and Materials, ASTM International, West Conshohocken, PA, 2008.

[38] W. Shen, Y. Wang, T. Zhang, M. Zhou, J. Li, X. Cui, Magnesia modification of alkali-activated slag fly ash cement, J. Wuhan Univ. Technol.-Mater. Sci. Ed. 26 (1) (2011) 121–125.

[39] BS E.N 12390–2:2009, Testing Hardened Concrete Part 3: Compressive Strength of test Specimens, BSI Standards Publication, 2009.

[40] ASTM C496-11, Standard Test Method for Splitting Tensile Strength of Cylindrical Concrete Specimens, ASTM International, West Conshohocken, PA, 2011.

[41] ASTM C78-16, Standard Test Method for Flexural Strength of Concrete (Using Simple Beam with Third-Point Loading), ASTM International, West Conshohocken, PA, 2016.

[42] ASTM C215-14, Standard Test Method for Fundamental Transverse, Longitudinal, and Torsional Resonant Frequencies of Concrete Specimens, ASTM International, West Conshohocken, PA, 2014.

[43] M. Talha Junaid, O. Kayali, A. Khennane, J. Black, A mix design procedure for low calcium alkali activated fly ash-based concretes, Constr. Build. Mater. 79 (2015) 301–310.

[44] F.A. Memon, M.F. Nuruddin, S. Khan, N. Shafiq, T. Ayub, Effect of sodium hydroxide concentration on fresh properties and compressive strength of self-compacting geopolymer concrete, J. Eng. Sci. Technol. 8 (1) (2013) 44–56.

[45] P.S. Deb, P. Nath, P.K. Sarker, Drying shrinkage of slag blended fly ash geopolymer concrete cured at room temperature, Procedia Eng. 125 (2015) 594–600.

[46] ASTM C403-08, Standard test method for time of setting of concrete mixtures by penetration resistance, American Society for Testing and Materials, Book of Standards, West Conshohocken, PA, 2008.

[47] BS EN 197-1:2011, Cement Part 1: Composition, Specifications and Conformity Criteria for Common Cements, BSI Standards Publication, 2011.

[48] A.A. Siyal, K.A. Azizli, Z. Man, H. Ullah, Effects of parameters on the setting time of fly ash based geopolymers using taguchi method, Procedia Eng. 148 (2016) 302–307.

[49] A. Rafeet, R. Vinai, M. Soutsos, W. Sha, Guidelines for mix proportioning of fly ash/GGBS based alkali activated concretes, Constr. Build. Mater. 147 (2017) 130–142.

[50] E. Gomaa, S. Sargon, C. Kashosi, M. ElGawady, Fresh Properties and Early Compressive Strength of Alkali-Activated High Calcium Fly Ash Paste, Singapore, Springer Singapore, 2018, pp. 497–507.

[51] ACI M318-05, Building Code Requirements for Structural Concrete and Commentary, American Concrete Institude, 2005.

[52] R.R. Lloyd, J.L. Provis, J.S.J. van Deventer, Microscopy and microanalysis of inorganic polymer cements. 1: remnant fly ash particles, J. Mater. Sci. 44 (2) (2009) 608–619.

[53] D. Hou, Z. Li, T. Zhao, Reactive force field simulation on polymerization and hydrolytic reactions in calcium aluminate silicate hydrate (C-A-S-H) gel: structure, dynamics and mechanical properties, RSC Adv. 5 (1) (2015) 448–461.

[54] X. Wan, D. Hou, T. Zhao, L. Wang, Insights on molecular structure and micro-properties of alkali-activated slag materials: A reactive molecular dynamics study, Constr. Build. Mater. 139 (2017) 430–437.

[55] J.L. Provis, A. Palomo, C. Shi, Advances in understanding alkali-activated materials, Cem. Concr. Res. 78 (Part A) (2015) 110–125.

[56] I. García-Lodeiro, A. Fernández-Jiménez, A. Palomo, Variation in hybrid cements over time Alkaline activation of fly ash-portland Cement blends, Cem. Concr. Res. 52 (2013) 112–122.

[57] G.S. Ryu, Y.B. Lee, K.T. Koh, Y.S. Chung, The mechanical properties of fly ash-based geopolymer concrete with alkaline activators, Constr. Build. Mater. 47 (2013) 409–418.

[58] B. En, 1–2: 2004 Eurocode 2: Design of Concrete Structures-Part 1–2: General Rules-Structural fire Design, European Standards, London, 2004.

[59] M. Sofi, J.S.J. van Deventer, P.A. Mendis, G.C. Lukey, Engineering properties of inorganic polymer concretes (IPCs), Cem. Concr. Res. 37 (2) (2007) 251–257.

[60] E.N.A.E. Ivan Diaz-Loya, V. Saiprasad, Mechanical properties of fly-ash-based geopolymer concrete, Mater. J. 108 (3) (2011) 300–306.

[61] CEB-FIP Model Code, Comite Euro-International Du Beton, 1995, p. 46.

[62] British Standard Institute, Structural Use of Concrete-Part 2: Code of Practice for Special Circumstance. BS 8110-2:1995, BSI, London, UK, 1985.

[63] Y. Zhou, J. Gao, Z. Sun, W. Qu, A fundamental study on compressive strength, static and dynamic elastic moduli of young concrete, Constr. Build. Mater. 98 (2015) 137–145.

[64] T. Noguchi, F. Tomosawa, K.M. Nemati, B.M. Chiaia, A.P. Fantilli, A practical equation for elastic modulus of concrete, ACI Mater. J. 106 (5) (2009) 690–696.